

## Partitioning hazy images using interactive active contour models

Firhan Azri Ahmad Khairul Anuar<sup>1</sup>, Jenevy Jone<sup>2</sup>, Raja Farhatul Aiesya Raja Azhar<sup>3</sup>,  
Abdul Kadir Jumaat<sup>1,4</sup>

<sup>1</sup>Faculty of Computer and Mathematical Sciences, Universiti Teknologi MARA, Shah Alam, Malaysia

<sup>2</sup>Finance Risk Cost Control, Shangri-La Rasa Ria, Pantai Dalit Tuaran, Kinabalu, Malaysia

<sup>3</sup>Faculty of Computing and Informatics, Universiti Malaysia Sabah, Kinabalu, Malaysia

<sup>4</sup>Institute for Big Data Analytics and Artificial Intelligence (IBDAAI), Universiti Teknologi MARA, Shah Alam, Malaysia

### Article Info

#### Article history:

Received Mar 14, 2025

Revised Oct 16, 2025

Accepted Oct 16, 2025

#### Keywords:

Active contour

Hazy grayscale image

Image partitioning

Segmentation

Variational level set

### ABSTRACT

Image partitioning, also known as image segmentation, is a process that involves dividing an image into distinct and meaningful segments. Recently, an interactive active contour model (ACM) namely the Gaussian regularization selective segmentation (GRSS) was designed to handle images with intensity inhomogeneity effectively. However, the GRSS model shows limited performance when applied to hazy images, which often results in incomplete detection and inaccurate extraction of the target object. This study reformulates the GRSS model by integrating the simple dark channel prior (SimpleDCP) dehazing technique, producing a modified model referred to as GRSS with SimpleDCP (GRSSD). The model is derived and implemented in MATLAB software. Experimental results show that the GRSSD model achieves improved segmentation accuracy (ACU) compared with the GRSS model. On average, the ACU improved by 1.8%, while the error metric (EM) decreased from 0.053 to 0.036, representing a reduction of about 32%. The Dice and Jaccard indices improved by approximately 2.6% and 4.9%, respectively. Although the computation time increased, the enhancement in segmentation ACU demonstrates the benefit of incorporating a dehazing process into the variational formulation. The proposed GRSSD model can be extended to color and three-dimensional image segmentation in future work.

This is an open access article under the [CC BY-SA](#) license.



### Corresponding Author:

Abdul Kadir Jumaat

Faculty of Computer and Mathematical Sciences, Universiti Teknologi MARA

Kompleks Al-Khawarizmi, 40450 Shah Alam, Selangor, Malaysia

Email: [abdulkadir@tmsk.uitm.edu.my](mailto:abdulkadir@tmsk.uitm.edu.my)

## 1. INTRODUCTION

Image processing is the process of interpreting and applying a digital image to gain information from it by making it clearer or more practical to observe. There are various types of image processing such as image dehazing and image partitioning, also known as image segmentation. Image partitioning is the process of segmenting an image into a specific object or region for further processing that can be applied in medical image analysis [1]–[5], pattern recognition, image understanding, and computer vision [6], [7]. Image partitioning is classified into two types: nonvariational image segmentation and variational image segmentation.

In the non-variational model category, image segmentation techniques are typically executed using a learning-based methodology such as deep learning and convolutional neural networks [8]. These methods

have demonstrated superior accuracy (ACU) in image segmentation. Deep learning is a prominent research trend in the advancement of artificial intelligence and machine learning. However, the learning-based methodology possesses specific shortcomings, including excessive reliance on data. To enhance output ACU, the method must utilize thousands of data points. Retrieving such a substantial amount of data within a limited timeframe is arduous. The variational model, especially the active contour model (ACM) is less dependent on the amount of data, less sensitive to noise and has a lot of features compared to the non-variational model mentioned above. ACMs are effective in generating high image segmentation quality and are very effective in extracting similar areas [9]. The ACMs have been widely applied in various fields of image analysis, including pattern recognition, and computer vision [10], [11]. These models are generally classified into two main categories: global segmentation and interactive segmentation [12].

The global segmentation approach seeks to divide the entire image into multiple regions based on features such as intensity, color, or texture distribution. This method is often suitable for cases where the object of interest occupies a significant portion of the image or when the global image characteristics are uniform. Examples of global segmentation models have been presented in the studies by [7], [13]–[16], where region-based energy formulations are utilized to achieve segmentation across the entire image domain. On the other hand, interactive or selective segmentation focuses on isolating specific objects or regions of interest through user guidance [17]. In this approach, the user provides initial input in the form of markers or seed points that indicate the approximate location of the target region. The segmentation algorithm then evolves the contour around these user-defined markers to accurately delineate the desired object. It has been effectively used in several application areas, including biomedical image analysis, pattern recognition, and document or text segmentation. Models proposed in [18]–[21] represent examples of interactive segmentation methods that depend on active user participation to achieve reliable results. The interaction enables the segmentation process to focus on the specific region of interest, thereby minimizing the influence of irrelevant image areas.

More recently, a model known as Gaussian regularization selective segmentation (GRSS) was developed. As an interactive ACM, this model was introduced to address challenges related to intensity inhomogeneity, where conventional models often fail to maintain consistent segmentation boundaries. Although the GRSS model performs effectively for images with nonuniform intensity, it shows limitations when applied to hazy images. Haze introduces visual degradation caused by the scattering of light by atmospheric particles such as dust, smoke, and aerosols, which reduces contrast and obscures object boundaries [22]. Consequently, accurate segmentation of hazy images becomes difficult without prior image enhancement. Dehazing techniques such as the simple dark channel prior (SimpleDCP) [23] have proven useful in improving image clarity and contrast, thereby facilitating more reliable feature extraction.

In this study, an improved formulation of the GRSS model is proposed by incorporating the SimpleDCP method into the variational framework. The resulting model, referred to as GRSS with SimpleDCP (GRSSD), is designed to enhance the segmentation ACU of hazy images by combining dehazing and variational principles. The structure of this paper is as follows: section 2 describes the methodology of the proposed model, section 3 presents the experimental results and discussion, and section 4 concludes the study with remarks and future research directions.

## 2. METHOD

This section presents the methods adopted for developing the GRSSD model. The overall process is outlined to provide a clear description of how the mathematical formulation is applied to image dehazing and segmentation. Figure 1 depicts the workflow of the four main phases undertaken in this study namely data acquisition, model formulation, algorithm development and performance evaluation. A detailed explanation of each phase is described in the next subsection.

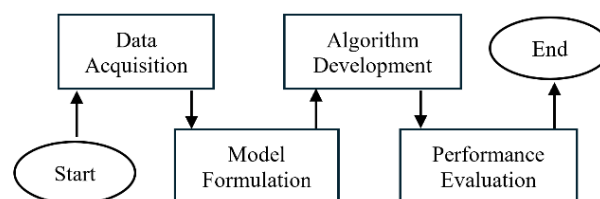


Figure 1. The research methodology

## 2.1. Data acquisition

Real test images were obtained from [24]–[28]. Benchmark images from the same sources were also used to ensure a consistent basis for model comparison and evaluation. All images were resized to 256×256 pixels using MATLAB R2023a to maintain uniform input dimensions for experimentation.

## 2.2. Model formulation

The second phase focuses on model formulation. In this stage, the GRSS model, recently introduced by [12], serves as the foundation for the proposed work. The GRSS model employs geometrical constraint  $A$ , also known as marker set which is placed near the object of interest. These markers guide the segmentation process by influencing the contour evolution within the image domain. Then, the GRSS model [12] is given as,

$$\min \left\{ GRSS = \frac{1}{2} \int_D (z_0 - (f_1 H(\phi) + f_2 (1 - H(\phi))))^2 dD + \theta \int_D P_d H(\phi) dD \right\} \quad (1)$$

Here, the function  $H(\phi)$  is the Heaviside function, the term  $\int_D P_d H(\phi) dD$  is the distance function weighted by the parameter  $\theta$  and the first term is the fitting term.

The GRSS model is designed to segment objects effectively into images with intensity in homogeneity. The contour generated from the segmentation process can be interactively adjusted by specifying appropriate positions for the marker set  $A$ , which serves as a geometrical constraint near the target object. However, the performance of the GRSS model decreases when applied to hazy images. Haze introduces visual degradation caused by the scattering of light by atmospheric particles. These particles reduce image contrast and clarity, making object boundaries less distinguishable and therefore more difficult to extract accurately during segmentation.

To mitigate the effects of haze, image dehazing methods such as the SimpleDCP [27] are commonly employed. The formation of a hazy image can be represented as,

$$Z_0(x, y) = J(x, y)T(x, y) + A(1 - T(x, y)) \quad (2)$$

Here,  $Z_0$  denotes the image with haze,  $J$  represents the scene radiance corresponding to the clean image,  $A$  is the global atmospheric light and  $T$  represents the transmission map. The clean image  $J$  can be represented using the relation,

$$J(x, y) = (Z_0(x, y) - A) / (\max(T(x, y), T_0)) + A \quad (3)$$

By combining these principles, a new interactive ACM is proposed to partition hazy images. The reformulated model integrates the dehazed image obtained from the SimpleDCP method into the existing GRSS framework. This enhanced formulation, referred to as the GRSS with SimpleDCP (GRSSD) model, incorporates haze removal into the variational segmentation process to achieve more reliable boundary extraction in degraded visual conditions is defined as follows,

$$\min \left\{ GRSSD = \frac{\alpha_1}{2} \int_D (J - (g_1 H + g_2 (1 - H)))^2 dD + \theta \int_D P_d H dD + \frac{\alpha_2}{2} \int_D Z_0 - (h_1 H + h_2 (1 - H))^2 dD \right\} \quad (4)$$

Where  $Z_0$  denotes the image with haze and  $J$  is the clean image computed using SimpleDCP. The first term weighted by  $\alpha_1$  is introduced to ensure the segmentation contour is approximately similar with the boundaries of the targeted object based on the haze free image from SimpleDCP method. This term is balanced with the third term which is weighted by  $\alpha_2$ , introduced to ensure the segmentation contour is approximately similar with the boundaries of the targeted object based on the original hazy image. The terms  $h_1(x, y) = k_\sigma * [H(\phi)Z_0] / k_\sigma * H(\phi)$  and  $g_1(x, y) = k_\sigma * [H(\phi)J] / k_\sigma * H(\phi)$  are the average of image intensities inside segmentation contour of  $Z_0$  and  $J$  respectively. The terms  $h_2(x, y) = k_\sigma * [1 - H(\phi)Z_0] / k_\sigma * [1 - H(\phi)]$  and  $g_2(x, y) = k_\sigma * [1 - H(\phi)J] / k_\sigma * [1 - H(\phi)]$  indicates the average of image intensities outside the segmentation contour of  $Z_0$  and  $J$  respectively.

In (4) is minimized using calculus of variation to obtain the (5),

$$-\delta(\phi) \{ \alpha_1 [J - g_1 H(\phi) - g_2 (1 - H(\phi))] (g_1 - g_2) + \alpha_2 [Z_0 - h_1 H(\phi) - h_2 (1 - H(\phi))] (h_1 - h_2) - \theta P_d \} \quad (5)$$

Based on the gradient descent method, (5) is written as (6).

$$\begin{aligned} \frac{\partial \phi}{\partial t} = & \delta(\phi) \{ \alpha_1 [J - g_1 H(\phi) - g_2 (1 - H(\phi))] (g_1 - g_2) + \\ & \alpha_2 [Z_0 - h_1 H(\phi) - h_2 (1 - H(\phi))] (h_1 - h_2) - \theta P_d \} \end{aligned} \quad (6)$$

An algorithm is developed in the next section to solve (6).

### 2.3. Algorithm development

The third phase comprises algorithm development, in which the mathematical model is implemented in MATLAB. The algorithm integrates the necessary computational steps for both dehazing and selective segmentation, following the derived variational formulation. The segmentation process will stop automatically if the solution reach  $tol = 1 \times 10^{-6}$  or the maximum number of iterations,  $maxit=100$ . The Algorithm 1 demonstrates the partitioning process using the proposed GRSSD model.

**Algorithm 1.** Algorithm to partition an image using the GRSSD model

```
1. Define the value of all parameters and compute dehazed image,  $J$  using (3).
>>  $J = imreducehaze(Image\_with\_haze);$ 
2. Set the coordinate of the marker set  $A$ .
>>  $c\_x = [a;b;c;d];$  >>  $c\_y = [e;f;g;h];$ 
3. Set  $\phi$  at  $t=0$ .
>>  $\phi = distance(c\_x, c\_y);$ 
4. For  $iteration=1$  to  $maxit$  or  $\frac{\|\phi^{k+1}-\phi^k\|}{\|\phi^k\|} \leq tol$  do
Solve (6).
Smooth  $\phi$  by computing  $\phi * k_\sigma$ .
>>  $phi = \phi * k_\sigma$ 
end for
```

### 2.4. Performance evaluation




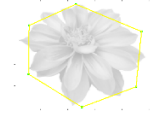


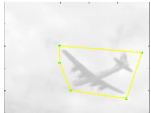





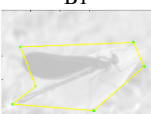


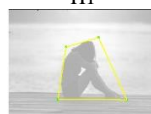


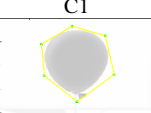
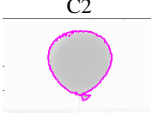
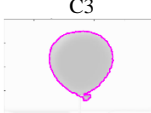
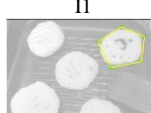


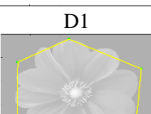
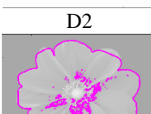


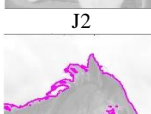
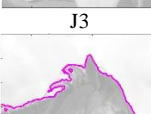

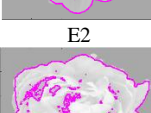

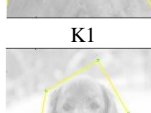
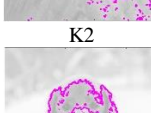
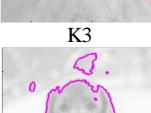
The performance of the proposed model was evaluated in terms of segmentation ACU and computational efficiency. Four quantitative indicators were employed: ACU, error metric (EM), Jaccard index, and Dice COEFFICIENT. The ACU was calculated using the expression  $ACU = (TP+TN)/(TP+FN+FP+TN)$  where true positive (TP) denotes the number of pixels correctly classified as belonging to the object of interest, and true negative (TN) represents the number of pixels correctly identified as background. Conversely, false positive (FP) refers to pixels incorrectly identified as part of the object, and false negative (FN) denotes pixels incorrectly excluded from the object region. A higher ACU value approaching one indicates greater segmentation ACU.

The relationship between ACU and EM is given by  $EM=1-ACU$ . This implies that when ACU increases, the corresponding error value decreases. Hence, a model that yields a high ACU typically exhibits a low EM value, indicating a strong agreement between the segmented output and the reference image. The similarity between the segmented region and the reference mask was further evaluated using the Jaccard and Dice coefficients, defined as  $Jaccard = |S_n \cap S_*| / |S_n \cup S_*|$  and  $Dice = |S_n \cap S_*| / (|S_n| + |S_*|)$  where  $S_n$  represents the set of pixels in the segmented output and  $S_*$  denotes the corresponding set in the ground truth. Both indices yield values between 0 and 1, where a value closer to one reflects a higher level of segmentation consistency and overlap with the ground truth. The computational efficiency of the proposed GRSSD model was also assessed by measuring its processing time. All experiments were carried out on a computer equipped with an AMD Ryzen 7 5700X processor, an Nvidia GeForce 1070 GPU, and 32 GB of RAM, operating at 3.80 GHz.

## 3. RESULTS AND DISCUSSION

An experiment was conducted to measure the performance GRSS model [12] and the new GRSSD model based on four quantitative measures: EM, ACU, Jaccard, and Dice indices, with reference to the benchmark datasets from [24]–[28]. The parameters setting are as follows:  $\alpha_1, \alpha_2 = [0.5, 10]$ ,  $tol=10^{-6}$ ,  $maxit=100$ ,  $\theta = 80$ . In practice,  $\alpha_1 > \alpha_2$  if input images containing haze and  $\sigma = [10, 200]$ . These parameter settings were applied consistently across all experiments to ensure a fair comparison between models. Table 1 summarized the visual results obtained under these configurations.

Table 1. Image partitioning results

Input images	GRSS model	GRSSD model	Input images	GRSS model	GRSSD model
					
A1	A2	A3	G1	G2	G3
					
B1	B2	B3	H1	H2	H3
					
C1	C2	C3	I1	I2	I3
					
D1	D2	D3	J1	J2	J3
					
E1	E2	E3	K1	K2	K3
					
F1	F2	F3	L1	L2	L3

In Table 1, the first and fourth columns display the hazy input images (A1–L1) that contain the target objects for segmentation. The regions of interest are marked with green indicators and a yellow initial contour. The second and fifth columns present the segmentation outcomes generated by the GRSS model, while the third and sixth columns show the corresponding results obtained using the proposed GRSSD model. Both models were able to delineate the target regions, as illustrated in Table 1(1b–12b) for the GRSS model and Table 1(1c–12c) for the GRSSD model. Visual examination, however, indicates that several results produced by the GRSS model demonstrate partial over-segmentation, particularly in images F2, G2, H2, and K2 of Table 1. This behavior occurs because the GRSS model has limited capability to manage the haze effect within the image, leading to less accurate boundary detection.

The results obtained from the GRSSD model show more distinct object boundaries and better separation between the object and background. The improvement is mainly due to the incorporation of the SimpleDCP method [27], which reduces the haze level in the input test image prior to the partitioning process. The dehazing step enhances image contrast and visibility, allowing the level set evolution to converge more accurately to the object boundary. Consequently, the GRSSD model provides segmentation results that are visually clearer and more stable across different image conditions. The corresponding quantitative evaluations were computed to validate the visual findings, while the partitioning process time was logged to assess computational efficiency. The numerical outcomes are summarized in Table 2.

Quantitative analysis based on Table 2 further validates the performance of the proposed GRSSD model compared to the existing GRSS model. The GRSSD model consistently demonstrates significant improvements across all performance metrics. On average, the ACU value increased from 0.947 to 0.964, which represents an improvement of approximately 1.8%, while the EM decreased from 0.053 to 0.036, equivalent to a reduction of about 32%. This reduction in error indicates that the GRSSD model provides a more precise segmentation of target regions, especially in images affected by haze. Similarly, the Dice similarity coefficient (DSC) improved from 0.884 to 0.907, showing an enhancement of approximately 2.6%, and the Jaccard similarity coefficient (JSC) increased from 0.800 to 0.839, indicating an improvement of about 4.9%. These quantitative gains are consistent with the visual observations presented in Table 1, confirming that the proposed model can more accurately delineate object boundaries and preserve structural details even under reduced visibility conditions.

Table 2. Values of ACU, EM, Dice, Jaccard, and time

Test image	ACU		EM		Dice		Jaccard		Time	
	GRSS	GRSSD	GRSS	GRSSD	GRSS	GRSSD	GRSS	GRSSD	GRSS	GRSSD
1	0.957	0.964	0.043	0.037	0.872	0.893	0.773	0.807	7.550	11.930
2	0.959	0.960	0.041	0.040	0.726	0.734	0.570	0.580	7.760	11.190
3	0.923	0.922	0.077	0.078	0.740	0.740	0.587	0.587	7.540	11.300
4	0.991	0.994	0.009	0.006	0.972	0.982	0.945	0.965	7.300	12.600
5	0.956	0.967	0.044	0.033	0.957	0.967	0.917	0.937	22.600	41.500
6	0.907	0.963	0.093	0.037	0.916	0.968	0.845	0.938	19.590	34.820
7	0.927	0.976	0.073	0.024	0.924	0.976	0.859	0.953	19.730	34.790
8	0.952	0.972	0.048	0.028	0.927	0.958	0.864	0.919	19.200	35.770
9	0.980	0.980	0.020	0.020	0.910	0.910	0.835	0.835	4.880	6.130
10	0.987	0.987	0.013	0.013	0.899	0.897	0.816	0.814	3.910	4.330
11	0.956	0.963	0.044	0.037	0.959	0.966	0.921	0.933	19.100	35.620
12	0.872	0.922	0.129	0.078	0.806	0.891	0.675	0.801	8.800	13.120
Average	0.947	0.964	0.053	0.036	0.884	0.907	0.800	0.839	12.330	21.092

The improvement in segmentation performance can be attributed to the incorporation of the SimpleDCP dehazing technique within the variational selective segmentation framework. The dehazing component enhances the contrast and visibility of hazy images, allowing the level set evolution to converge more effectively towards true object boundaries. As a result, the model becomes more robust to intensity degradation and haze-induced blurring, which typically challenge traditional active contour formulations. Although the inclusion of the dehazing term increases computational complexity, resulting in a longer average processing time from 12.33 seconds to 21.09 seconds, this represents an acceptable trade-off considering the substantial improvements in segmentation ACU and reliability. Overall, the quantitative and qualitative analyses collectively demonstrate that the proposed GRSSD model outperforms the GRSS model in both ACU and robustness. The incorporation of the dehazing process into the active contour formulation significantly improves segmentation precision, particularly for hazy or low-contrast images.

#### 4. CONCLUSION

The GRSS model was reformulated to address image partitioning in hazy environments by integrating the SimpleDCP dehazing technique to produce a modified model referred to as GRSSD. The proposed GRSSD model was derived using the calculus of variations and implemented on real image datasets in MATLAB software. The model performance was evaluated using four quantitative measures, namely ACU, EM, Dice, and Jaccard indices.

The findings show that the GRSSD model achieved improved segmentation ACU compared with the original GRSS model. On average, the ACU value increased from 0.947 to 0.964, representing an improvement of approximately 1.8%, while the EM value decreased from 0.053 to 0.036, corresponding to a reduction of about 32%. Similarly, the Dice coefficient improved from 0.884 to 0.907, and the Jaccard index increased from 0.800 to 0.839, reflecting relative gains of 2.6% and 4.9%, respectively. These improvements indicate that the dehazing process contributed to better contrast and clearer boundary definition, leading to more accurate segmentation results in hazy conditions.

Although the inclusion of the dehazing term increased computational cost, with the average processing time rising from 12.330 seconds to 21.092 seconds, the enhancement in segmentation precision justifies this trade-off. The results demonstrate that combining dehazing and variational segmentation methods can improve the reliability of image analysis under challenging visual conditions. The proposed method has potential applications in several domains, including object tracking, autonomous vehicle systems, and traffic monitoring. Future research will aim to develop a more efficient optimization scheme to enhance computational performance and to extend the current model for use in color images and three-dimensional segmentation tasks.

#### ACKNOWLEDGMENTS

The authors would like to express their sincere appreciation to Universiti Teknologi MARA (UiTM) for the support provided in the completion of this research.

#### FUNDING INFORMATION

This research received no specific grant from any funding agency in the public, commercial, or not-for-profit sectors.



## AUTHOR CONTRIBUTIONS STATEMENT

This journal uses the Contributor Roles Taxonomy (CRediT) to recognize individual author contributions, reduce authorship disputes, and facilitate collaboration.

Name of Author	C	M	So	Va	Fo	I	R	D	O	E	Vi	Su	P	Fu
Firhan Azri Ahmad	✓	✓	✓	✓	✓	✓		✓	✓	✓	✓			
Khairul Anuar														
Jenevy Jone	✓	✓	✓	✓	✓	✓		✓	✓	✓	✓			
Raja Farhatul Aiesya	✓	✓	✓	✓	✓	✓		✓	✓	✓	✓			
Raja Azhar														
Abdul Kadir Jumaat	✓	✓	✓	✓			✓	✓		✓		✓	✓	✓

C : Conceptualization

M : Methodology

So : Software

Va : Validation

Fo : Formal analysis

I : Investigation

R : Resources

D : Data Curation

O : Writing - Original Draft

E : Writing - Review & Editing

Vi : Visualization

Su : Supervision

P : Project administration

Fu : Funding acquisition

## CONFLICT OF INTEREST STATEMENT

Authors declare that they have no known competing financial interests or personal relationships that could have appeared to influence the work reported in this paper. Authors state no conflict of interest.

## DATA AVAILABILITY

The data that support the findings of this study are openly available in references [24]-[28].




## REFERENCES

- [1] F. A. Shewajo and K. A. Fante, "Tile-based microscopic image processing for malaria screening using a deep learning approach," *BMC Medical Imaging*, vol. 23, no. 1, 2023, doi: 10.1186/s12880-023-00993-9.
- [2] A. M. Anter and L. Abualigah, "Deep federated machine learning-based optimization methods for liver tumor diagnosis: a review," *Archives of Computational Methods in Engineering*, vol. 30, no. 5, pp. 3359–3378, 2023, doi: 10.1007/s11831-023-09901-4.
- [3] S. Srinivasan, P. S. M. Bai, S. K. Mathivanan, V. Muthukumaran, J. C. Babu, and L. Vilcekova, "Grade classification of tumors from brain magnetic resonance images using a deep learning technique," *Diagnostics*, vol. 13, no. 6, 2023, doi: 10.3390/diagnostics13061153.
- [4] Z. Q. Habeeb, B. Vuksanovic, and I. Q. Al-Zaydi, "Breast cancer detection using image processing and machine learning," *Journal of Image and Graphics(UK)*, vol. 11, no. 1, pp. 1–8, 2023, doi: 10.18178/joig.11.1.1-8.
- [5] I. Mishra, K. Aravinda, J. A. Kumar, C. Keerthi, R. Divya Shree, and S. Srikumar, "Medical imaging using signal processing: a comprehensive review," *Proceedings of the 2nd International Conference on Artificial Intelligence and Smart Energy, ICAIS 2022*, pp. 623–630, 2022, doi: 10.1109/ICAIS53314.2022.9742778.
- [6] M. I. Yeşil and S. Göncü, "Recognition of Hereford and Simmental cattle breeds via computer vision," *Iranian Journal of Applied Animal Science*, vol. 13, no. 1, pp. 21–32, 2023.
- [7] J. Fang, H. Liu, L. Zhang, J. Liu, and H. Liu, "Region-edge-based active contours driven by hybrid and local fuzzy region-based energy for image segmentation," *Information Sciences*, vol. 546, pp. 397–419, 2021, doi: 10.1016/j.ins.2020.08.078.
- [8] R. Yousef *et al.*, "U-Net-based models towards optimal MR brain image segmentation," *Diagnostics*, vol. 13, no. 9, 2023, doi: 10.3390/diagnostics13091624.
- [9] K. Chen, "Introduction to variational image-processing models and applications," *International Journal of Computer Mathematics*, vol. 90, no. 1, pp. 1–8, 2013, doi: 10.1080/00207160.2012.757073.
- [10] G.-L. Zhu, X.-G. Lv, F. Li, and X.-M. Sun, "Nonconvex variational approach for simultaneously recovering cartoon and texture images," *Journal of Electronic Imaging*, vol. 31, no. 04, 2022, doi: 10.1117/1.jei.31.4.043021.
- [11] X. Liu, G. Liu, Y. Wang, G. Li, R. Zhang, and W. Peng, "A variational level set image segmentation method via fractional differentiation," *Fractal and Fractional*, vol. 6, no. 9, 2022, doi: 10.3390/fractalfract6090462.
- [12] T. C. Saibin and A. K. Jumaat, "Variational selective segmentation model for intensity inhomogeneous image," *Indonesian Journal of Electrical Engineering and Computer Science (IJECS)*, vol. 29, no. 1, pp. 277–285, 2023, doi: 10.11591/ijeecs.v29.i1.pp277-285.
- [13] J. Gu, Z. Fang, Y. Gao, and F. Tian, "Segmentation of coronary arteries images using global feature embedded network with active contour loss," *Computerized Medical Imaging and Graphics*, vol. 86, 2020, doi: 10.1016/j.compmedimag.2020.101799.
- [14] Y. Yang, W. Jia, and B. Wu, "Simultaneous segmentation and correction model for color medical and natural images with intensity inhomogeneity," *Visual Computer*, vol. 36, no. 4, pp. 717–731, 2020, doi: 10.1007/s00371-019-01651-4.
- [15] E. Iqbal, A. Niaz, A. A. Memon, U. Asim, and K. N. Choi, "Saliency-driven active contour model for image segmentation," *IEEE Access*, vol. 8, pp. 208978–208991, 2020, doi: 10.1109/ACCESS.2020.3038945.
- [16] X. H. Zhi and H. Bin Shen, "Saliency driven region-edge-based top down level set evolution reveals the asynchronous focus in image segmentation," *Pattern Recognition*, vol. 80, pp. 241–255, 2018, doi: 10.1016/j.patcog.2018.03.010.
- [17] W. Zhao, W. Wang, X. Feng, and Y. Han, "A new variational method for selective segmentation of medical images," *Signal Processing*, vol. 190, 2022, doi: 10.1016/j.sigpro.2021.108292.
- [18] N. Badshah and K. Chen, "Image selective segmentation under geometrical constraints using an active contour approach," *Communications in Computational Physics*, vol. 7, no. 4, pp. 759–778, 2010, doi: 10.4208/cicp.2009.09.026.




- [19] L. Rada and K. Chen, "Improved selective segmentation model using one level-set," *Journal of Algorithms and Computational Technology*, vol. 7, no. 4, pp. 509–540, 2013, doi: 10.1260/1748-3018.7.4.509.
- [20] J. Spencer and K. Chen, "A convex and selective variational model for image segmentation," *Communications in Mathematical Sciences*, vol. 13, no. 6, pp. 1453–1472, 2015, doi: 10.4310/CMS.2015.v13.n6.a5.
- [21] A. K. Jumaat and K. Chen, "A reformulated convex and selective variational image segmentation model and its fast multilevel algorithm," *Numerical Mathematics*, vol. 12, no. 2, pp. 403–437, 2019, doi: 10.4208/nmtma.OA-2017-0143.
- [22] H. Ali, A. Sher, M. Saeed, and L. Rada, "Active contour image segmentation model with de-hazing constraints," *IET Image Processing*, vol. 14, no. 5, pp. 921–928, 2020, doi: 10.1049/iet-ipr.2018.5987.
- [23] D. Park, H. Park, D. K. Han, and H. Ko, "Single image dehazing with image entropy and information fidelity," *2014 IEEE International Conference on Image Processing, ICIP 2014*, pp. 4037–4041, 2014, doi: 10.1109/ICIP.2014.7025820.
- [24] V. T. Pham, "How to use detectron2," *github.com*, 2015. <https://github.com/facebookresearch/detectron2/issues/795> (accessed Feb. 05, 2024).
- [25] J. Li, J. Zhang, and D. Tao, "Deep automatic natural image matting," in *IJCAI International Joint Conference on Artificial Intelligence*, 2021, pp. 800–806, doi: 10.24963/ijcai.2021/111.
- [26] Y. Qiao *et al.*, "Attention-guided hierarchical structure aggregation for image matting," in *Proceedings of the IEEE Computer Society Conference on Computer Vision and Pattern Recognition*, 2020, pp. 13673–13682, doi: 10.1109/CVPR42600.2020.01369.
- [27] H. Li, J. Cai, T. N. A. Nguyen, and J. Zheng, "A benchmark for semantic image segmentation," 2013, doi: 10.1109/ICME.2013.6607512.
- [28] M. Y. Chen *et al.*, "Automatic Chinese food identification and quantity estimation," in *SIGGRAPH Asia 2012 Technical Briefs*, 2012, doi: 10.1145/2407746.2407775.

## BIOGRAPHIES OF AUTHORS






**Firhan Azri Ahmad Khairul Anuar**    is a student of B. Sc. degree in mathematics from Universiti Teknologi MARA (UiTM) Shah Alam. His research interests revolve around mathematical modeling and image processing. He can be contacted at email: 2023104939@student.uitm.edu.my.






**Jenevy Jone**    obtained her B.Sc. degree in mathematics from Universiti Teknologi MARA (UiTM) Shah Alam. She is currently working as a Finance Risk Cost Control Assistant at Shangri-La Rasa Ria, Kota Kinabalu. Her research interests revolve around mathematical modeling and image processing. She can be contacted at email: jenevyjone@gmail.com



**Raja Farhatul Aiesya Raja Azhar**    obtained her B.Sc. degree in mathematics from Universiti Teknologi MARA (UiTM) Shah Alam and is currently pursuing a Master of computer science (computational intelligence) at Universiti Malaysia Sabah. Her studies focus on computational intelligence techniques, including nature-inspired computing, artificial neural networks, and multi-objective optimization. Her research interests revolve around mathematical modeling and image processing. She can be contacted at email: aiesya77@yahoo.com.



**Abdul Kadir Jumaat**    obtained the B.Sc. and M.Sc. degrees in mathematics from the Universiti Teknologi MARA, (UiTM) Shah Alam, Malaysia and the University of Liverpool, in United Kingdom, awarded him a Ph.D. degree particularly in applied mathematics (mathematical imaging methods). Presently, he holds the position of senior lecturer at the School of Mathematical Sciences, College of Computing, Informatics and Mathematics and a research fellow at the Institute for Big Data Analytics and Artificial Intelligence (IBDAAI) in UiTM Shah Alam, Malaysia. His research interests encompass various fields such as image/signal processing, artificial intelligence, computer vision, biometrics, medical image and analysis, and pattern recognition. He can be contacted at email: abdulkadir@tmsk.uitm.edu.my.